Desalination and Water Treatment
www.deswater.com
doi: 10.5004/dwt.2023.29717

300 (2023) 167–177
July

Methylene blue removal using black cumin seeds waste: experimental study and molecular dynamic simulation

Faouzia Benamraoui[a], Hassina Boudiaf[a], Antar Bouhank[a], Lahcene Bencheikh[a], Riadh Bourzami[b], Antonio Gil[c], Aziza-Imène Boulahbal[c], Mokhtar Boutahala[a,*]

[a]*Laboratoire de Génie Chimique, Département de Génie des Procédés, Faculté de Technologie, Université Ferhat Abbas Sétif-1, 19000, Sétif, Algérie, emails: mboutahala@univ-setif.dz/mboutahala@yahoo.fr (M. Boutahala), ben_amraouif@yahoo.fr (F. Benamraoui), boudiafhassina2000@yahoo.fr (H. Boudiaf), antabouhank@yahoo.fr (A. Bouhank), bencheikh_lahcene@yahoo.com (L. Bencheikh)*
[b]*Laboratoire des Matériaux Polymériques et Multiphasiques, Département de Génie des Procédés, Faculté de Technologie, Université Ferhat Abbas Sétif-1, 19000, Sétif, Algérie, email: riadh_bourzami@hotmail.com (R. Bourzami)*
[c]*Département des Sciences, Bâtiment Los Acebos, Université Publique de Navarra, Campus de Arrosadía, 31006, Pamplona, Spain, emails: andoni@unavarra.es (A. Gil), boulahbal_imene@yahoo.com (A.I. Boulahbal)*

Received 21 March 2023; Accepted 15 June 2023

ABSTRACT

This study reports a potential valorization of black cumin seed waste (BSW) as a low-cost biosorbent for methylene blue (MB) removal. The developed sample was investigated using operational parameters (initial concentration, pH, temperature, adsorbant mass, ionic strength, and contact time) and characterization techniques (transmission electron microscopy, X-ray diffraction, thermogravimetric analysis, Fourier-transform infrared spectroscopy, pH_{PZC}, and N_2 adsorption/desorption isotherms). The pseudo-second-order and the Langmuir equations were the best-fitted models to indicate the uptake of MB dye, with an adsorption efficiency of 346.1 mg/g at 20°C. The thermodynamic results suggest that MB adsorption on BSW was favorable, spontaneous, and exothermic. The statistical physics model was used to determine the adsorption mechanism of MB onto the sample BSW. Additionally, the interaction between the MB molecules and the BSW was examined using the Monte Carlo simulation method. The adsorption energy of MB onto BSW was – 19.0 (kcal/mol), indicating the potential of the adsorbant toward MB dye. The primary mechanisms governing the adsorption process were hypothesized to be electrostatic attraction, van der Waals forces, and hydrogen bonding. Overall, BSW demonstrated promising potential as an alternative low-cost biosorbent for the efficient removal of MB dye from wastewater.

Keywords: Black cumin seed waste; Methylene blue adsorption; Molecular dynamic simulation

1. Introduction

Human beings and dyes have a long history that has spanned the ages until today [1]. As we all know, color is essential to modern life. Many industries use dyes to add color to their products, including dyes, textiles, paper, printing, plastics, food, pharmaceuticals and cosmetics [2]. These dyes give us bright colors, but they are routinely included in industrial wastes and then discharged into water bodies in general and seriously threaten the safety of life. The presence of residual dyes in effluents, even at low concentrations, not only produces visible and undesirable colors [3], but also affect the health of aquatic organisms and human beings. Synthetic dyes have a stable, aromatic and non-biodegradable molecular structure [4], which poses a significant threat to the environment and human

* Corresponding author.

health. Therefore, industrial effluents containing dyes must be treated before being released into the environment [5]. Methylene blue (MB), a basic cationic dye, is one of the most widely used synthetic dyes not only in the dyeing industry but also in the chemical, biological and medical sciences [6]. Some of the health problems caused by prolonged exposure to MB include allergy, nausea, respiratory problems and burning eyes, dizziness, jaundice and even dysfunction of the central nervous system, liver and brain [7]. Therefore, the removal of dyes from wastewater has become a major environmental concern [8]. In order to treat wastewater polluted by dyes, coagulation–flocculation, oxidation, membrane filtration, and adsorption processes have been widely proposed [9–11]. Dyes removal by adsorption has become popular as its simple to use, inexpensive and capable to remove low levels of dyes from water [12]. It is an efficient, economical method and leaves no toxicity or adverse effects in the water. One of the most common adsorbents is activated carbon (AC), which is widely used and has excellent characteristics for the removal of organic and inorganic substances in the adsorption process [13]. However, commercial activated carbons are considered expensive adsorbents because they are made from relatively expensive and non-renewable precursors like coal [14]. The high price of AC causes economic difficulties and limits the application of this adsorbent. In recent years, research into biomass waste as an alternative adsorbent, ecological, available, efficient and low-cost is receiving increasing attention from researchers. Some interesting biomass, which have been investigated as low-cost sorbents used for the removal of dyes are de-oiled soya [15], guava leaf powder [16], ash of black turmeric rhizome [17], platanus leaves [18], papaya stem [19], and banana leaves [20].

Nigella sativa seeds, also known as black cumin seeds (BCS), are inexpensive and non-toxic. It was a popular and commonly cultivated plant that originated in Southwest Asia, Southern Europe, and North Africa. They have been widely used in traditional medicine to relax inflammation, reduced cholesterol and blood tension, kill bacteria, protect the liver, control blood sugar, and protect stomach ulcers [21]. BCS contain traces of alkaloids as well as a variety of unsaturated fatty acid esters with unusual structures involving terpene alcohols [22] and are primarily composed of fiber, lipids, carbohydrates, ash, and proteins. Aside from that, the surface functions of black cumin seeds involve hydroxyl (OH), carbonyl (C=O), carboxyl (COOH), and amines (NH_2) groups, which can provide attractive sites for polar molecules and/or ions [23–26].

In this study, the black cumin seed waste (BSW) was investigated as a bioadsorbent for MB dye removal depending on operating conditions. Batch adsorption experiments were carried out to examine the effects of mass, initial dye concentrations, contact time, solution pH, inorganic salts, and temperature. The kinetics, isotherm, thermodynamic, and mechanism of MB adsorption on the BSW were also investigated. In addition, statistical physical and molecular dynamic simulation methods were employed to estimate the probable orientation and interactions between MB and surface of BSW to supplement the experimental study. This study has not been reported in the literature to our knowledge.

2. Experimental set-up

2.1. Materials and chemicals

The material used in this work is a waste product recovered after the biorefining of the raw material from the black cumin seeds obtained from a local market in Setif, Algeria. The black cumin seeds waste were washed several times with distilled water and dried in an oven at 80° for 24 h. It was crushed and sieved with a sieve with a pore size of 0.5 mm. This material was named BSW. The chemicals, MB ($C_{16}H_{14}N_3SCl{\cdot}3H_2O$, with a wavelength of maximum absorption; λ_{max} = 664 nm, and $P\% \geq 95$). NaOH and HCl are of analytical grade and were purchased from Sigma-Aldrich, Germany.

2.2. Characterization techniques

Desorption adsorption isotherms of N_2 gas were performed using the Micromeritics TriStar 3000 instrument at 77 K. Vacuum degassing of BSW was performed at 100°C/3 h. The specific surface area of the BSW sample was determined using the Brunauer–Emmett–Teller (BET) method at relative pressure in the range of 0.05–0.35 [27]. The total pore volume, V_{pore}, was directly determined from the nitrogen adsorption isotherm at $P/P_0 = 0.98$.

Fourier-transform infrared (FTIR) spectra of the BSW bioadsorbent before and after MB adsorption were taken using a Fourier-transform infrared spectrophotometer (IRAffinity-1S; Shimadzu UV-1700, Japan) in the wavenumber range of 4,000–400 cm^{-1} to determine the functional groups exist on the surface of the BSW and responsible for the adsorption phenomenon.

Thermogravimetric analysis (TGA/DSC) was performed using a SDTQ600 thermo-balance. The thermal evolution is performed from ambient temperature to 700°C, following a ramp of 10°C/min.

SEM (scanning electron microscopy) images of the surface morphology of the BSW sample before and after MB adsorption were obtained with the NEOSCOPE JEOL JCM-5000 instrument.

X-ray diffraction (XRD) was obtained by D8 ADVANCE diffractometer (Bruker) using Cu-Kα radiation, which produces X-rays of wavelength λ = 1.54 Å and the scanning was performed in the range of $2° \leq \theta \leq 80°$.

The method outlined by [28] was used to determine the point of zero charge (pH_{PZC}). Briefly, the initial pHs (pHi) of 0.01 M NaCl solutions (50 mL) were adjusted in the pH range of 2–12 using HCl or NaOH. After that, each solution received 0.2 g of biosorbent. The suspensions were stirred for 48 h at 25°C to determine the final pH (pHf) of the solutions. The pHf vs. pHi plot was applied to evaluate the zero charge point.

2.3. Adsorption tests

The MB dye stock solution was prepared and dilution was used to obtain solutions at the selected concentrations. The different experimental effects on adsorption were studied such as contact time (3–120 min), initial concentration of MB (7.8, 32.9, and 56.5 mg/L), dose of adsorbent (3–30 mg), effect of NaCl salt (0–10^{-1} mol/L) and pH

(2–12). The experiments were conducted by stirring 20 mL of MB dye solution in 50 mL with 20 mg of BSW sample under a speed of 200 rpm for 2 h at room temperature with pH = 6.4 of MB dye solution. The impact of temperature on the adsorption characteristics was examined at 20°C, 30°C and 40°C for 24 h. For the adsorption isotherm, the initial concentrations ranged between 10 and 500 mg/L under a rotation speed of 200 rpm for 24 h at 20°C. The initial and final concentrations of MB dye were determined using a UV/visible spectrophotometer (Shimadzu UV/Vis 1700, Japan) at 665 nm.

2.4. Error analysis

In this study, the statistical parameters, such as correlation coefficient R^2 and Akaike information criterion correction $AIC_{corrected}$ were used to evaluate the performance of the kinetic and isotherm models. It was performed using Origin Pro (2018) software [29].

$$R^2 = \frac{\sum\left(q_{mean} - q_{cal}\right)^2}{\sum\left(q_{cal} - q_{mean}\right)^2 + \sum\left(q_{cal} - q_{exp}\right)^2} \quad (1)$$

$$AIC_{corrected} = NLn\left[\frac{\sum\left(q_{exp} - q_{cal}\right)^2}{N}\right] + 2K + \frac{2K\left(K+1\right)}{N-K-1} \quad (2)$$

where q_{exp}, q_{cal} in (mg/g) are the experimental sorption capacities and the sorption capacities predicted by the models, respectively. K and N are the numbers of model parameters and data points, respectively.

2.5. Theoretical study

The interactions between the MB dye and the cellulose substrate was performed using chemical calculations. Indeed, these chemistry calculations were performed using three software packages; Gaussian 9.5 W based on DFT for the geometry optimizations of adsorbate molecules MB and water molecules, Forcite module based on classical theory for the geometrical optimizations of the cellulose and finally, based on Monte Carlo theory, the adsorption locator module performs the adsorption. For this last, a supercell (100) of cellulose with the dimensions (24.603 × 31.140 × 6.486 Å corresponding to 3 × 3 × 1 unit cells) was generated starting from the refined geometry of Nishiyama et al. [30], and the crystallographic parameters defined in chemical oxygen demand data base file N° 4114994. The detailed calculation parameters have been reported in our previous papers [31–33].

3. Results and discussion

3.1. Physico-chemical characterization

The N_2 adsorption/desorption isotherm of BSW at 77.4 K based on IUPAC standards; shows that the observed isotherm is type II with a type H3 hysteresis loop. It means that the adsorbent formed aggregates and can be attributed to capillary condensation occurring in a non-rigid texture and is not indicative of a specific mesoporosity [34]. The values of BSW's S_{BET}, V_{pore}, and D_p are 2.5 m^2/g, 0.0009 cm^3/g, and 14.1 nm, respectively.

The functional groups present onto BSW the surface can be determined using FTIR spectra. In Fig. 1, the broad band obtained at 3,431 cm^{-1} is due to the stretching vibrations of hydroxyl groups (O–H), carboxylic acids, phenol and alcohols indicating the presence of O–H groups on the adsorbent surface [35]. This band also characterizes the O–H stretching vibrations of cellulose, pectin, adsorbed water and lignin [36]. Peaks observed at 2,925; 2,855 and 1,710 cm^{-1} correspond to CH stretching of the $–CH_2$, $–CH_3$ groups [25] and carboxyl group –C=O stretching [37], respectively. While the bands observed at (1,640–1,551 cm^{-1}) were engendered by amide C=O and NH groups [25]. The peak at 1,044 cm^{-1} is related to C–O stretching vibrations of carboxylic, phenolic and alcoholic groups [28]; this band also confirms the lignin structure of BSW [38]. The peak at 600 cm^{-1} corresponds to the C–N stretching vibration [39]. After MB adsorption, the peaks are shifted to different wavelengths. Reductions in peak intensities during adsorption were also observed at (3,445–2,925 cm^{-1} – 2,852–1,645 cm^{-1}), and an increase in the intensity of the 675 cm^{-1} band attributed to N–H. These changes indicate possible interactions between functional groups on the BSW surface and MB^+ ions [40]. In addition, new peaks were observed around 3,854; 1,698 and 880 cm^{-1}, suggesting MB adsorption.

The thermal decomposition curve of BSW shows a first mass loss of 9.56% around 51.5°C corresponding to the loss of physiosorbed water (figure not shown). Then, two other exothermic peaks at 223°C and 318°C correspond to a loss of mass of 19.84% and 54.25%, respectively, due to an important decomposition of the carbon contained in the BSW structure [28]. The thermogram shows that BSW remains stable above 550°C and the total mass loss achieved is close to 84.91 wt.%.

In Fig. 2, the SEM analysis of BSW before and after MB adsorption is displayed. Before adsorption (Fig. 2a), the SEM images clearly indicate the surface roughness with heterogeneous morphology, in the presence of a diversity of cavities. These cavities can be described as channels on

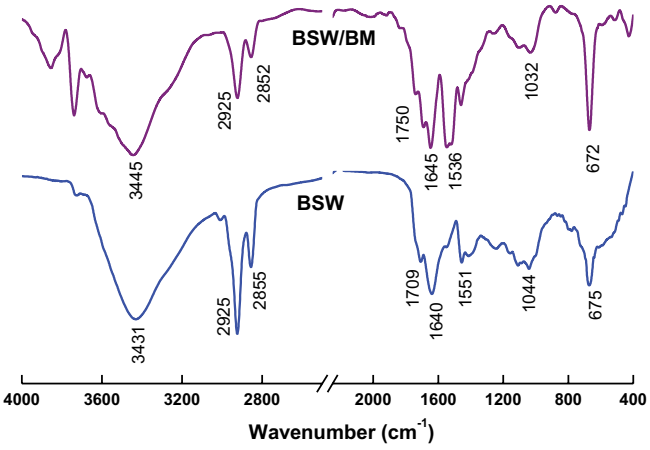

Fig. 1. Fourier-transform infrared spectra of black cumin seed waste: (a) before and (b) after methylene blue dye adsorption.

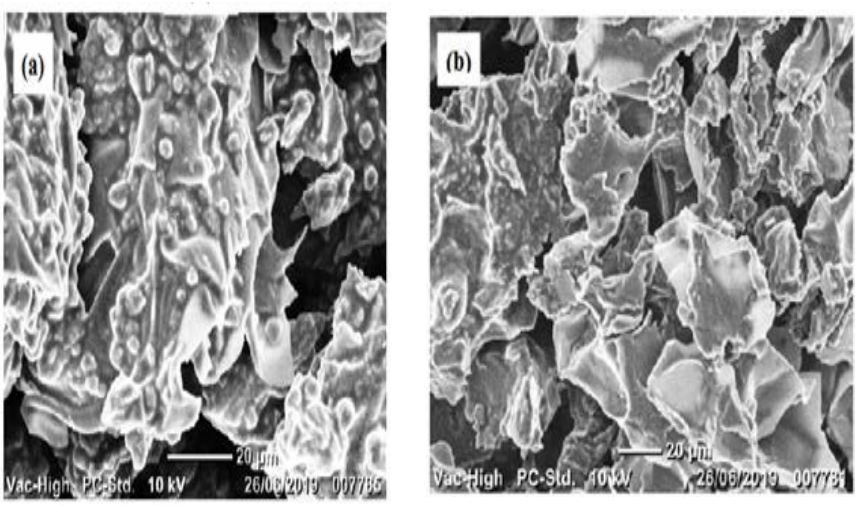

Fig. 2. Scanning electron microscopy of black cumin seed waste before (a) and after methylene blue adsorption (b).

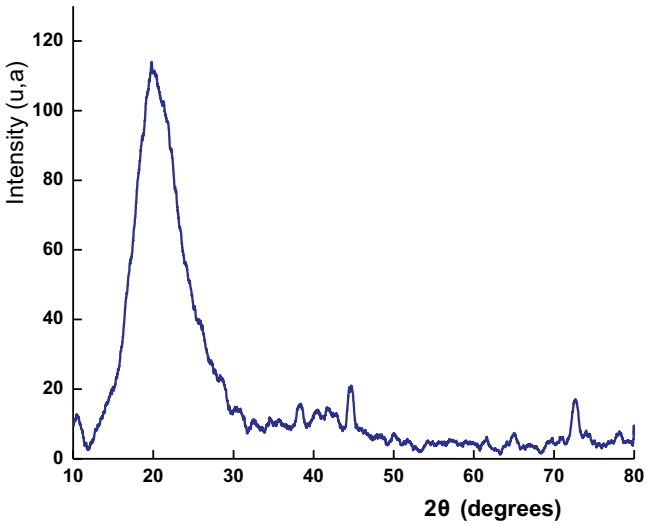

Fig. 3. X-ray diffraction pattern of black cumin seed waste.

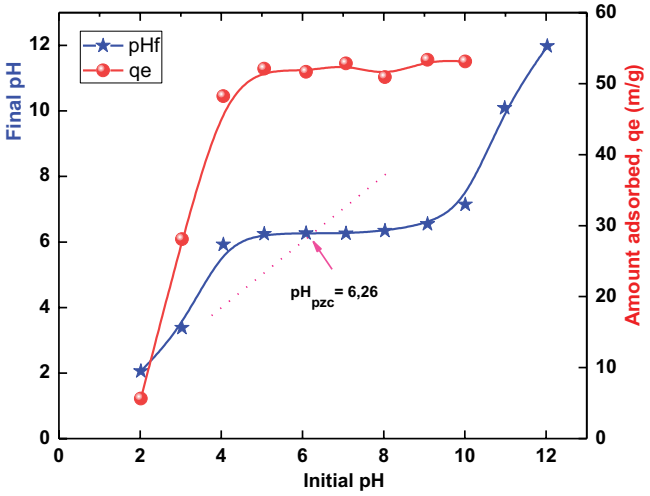

Fig. 4. The pH_{PZC} of the black cumin seed waste and the effect of initial pH on the removal of methylene blue onto black cumin seed waste.

the BSW surface, rather than pores. After dye adsorption (Fig. 2b), a smooth surface is observed, indicating the existence of interactions between MB and BSW.

The XRD spectrum of BSW is shown in Fig. 3. The broad peak in Fig. 3 between (2θ) 17° and 21° represents the cellulose content of the adsorbent [23]. The weak peaks are attributed to the amorphous nature of the adsorbent. The calculation of crystallite size for a crystalline material is given by the Scherrer equation [31].

$$D = \frac{0.9\lambda}{\beta\cos\theta} \tag{3}$$

where D is the size of the crystallite diameter, λ is the wavelength (k = 0.15405 nm for CuKα), β is the width at half height (FWHM) in radians, K = 0.9 is a constant, called the form factor related to the crystallite shape and θ is the diffraction angle in degrees. After calculation, we obtain a crystallite size close to 2.45 nm.

3.2. Effect of experimental conditions

Fig. 4 depicts the effect of pH. This figure shows that pH_{PZC} of BSW sample is close to 6.26. At pH below pH_{PZC}, the adsorption of MB^+ cations is disfavored because the surface is positively charged (SOH_2^+), whereas at pH above pH_{PZC}, the adsorption of MB^+ cations is favored because the surface is negatively charged (SO^-) due to electrostatic attraction [41]. When the solution pH is reduced from 5.06 to 2.02, the percentage removal of MB decreases from 92.8% (q_e = 52.1 mg/g) to 11.01% (q_e = 5.64 mg/g). This decrease can be explained by two factors: (i) an excess of H^+ protons competing with MB^+ cations for acidic adsorption sites, and (ii) an increase in the density of positive charges on the adsorbent surface increases repulsions with MB^+ cations [42].

The effect of initial concentration on adsorption was tested for a range of initial concentration from 20 to 560 mg/L (Fig. 5). It is observed that the quantity of MB adsorbed at

equilibrium (q_e) increases from 20.82 to 297.68 mg/g with increasing initial dye concentration, due to the increased likelihood of contact between BSW active sites and MB dye. This improves the resistance to mass transfer between the BSW and liquid phases [43]. However, at low initial concentration, the percentage of MB removal is high, but it decreases from 91.88% to 53.40% with increasing initial concentration. More MB molecules would rapidly saturate the active sites on BSW surface at higher dye concentration. Due to the limited number of adsorption sites, the percentage removal decreases [44].

In order to find an appropriate solid-to-liquid ratio, the effect of adsorbent dosage on MB ion removal was investigated. In this study, BSW doses ranging from 3 to 30 mg were used. Fig. 6 shows the results of the effect of BSW mass in terms of the amount adsorbed (q_e) and percent removal (% R) of MB. This figure shows that the adsorption efficiency increases from 83.83% to 94.53% when the dose of adsorbent increases from 3 to 30 mg, due to the increase in S_{BET} and therefore more adsorption sites are available on BSW surface [9]. Similarly, the adsorbed amount q_e of adsorbed MB dye decreases from 160.74 to 18.09 mg/g with the increase in adsorbent dose. In this study, a dose of 20 mg of adsorbent was used for all tests.

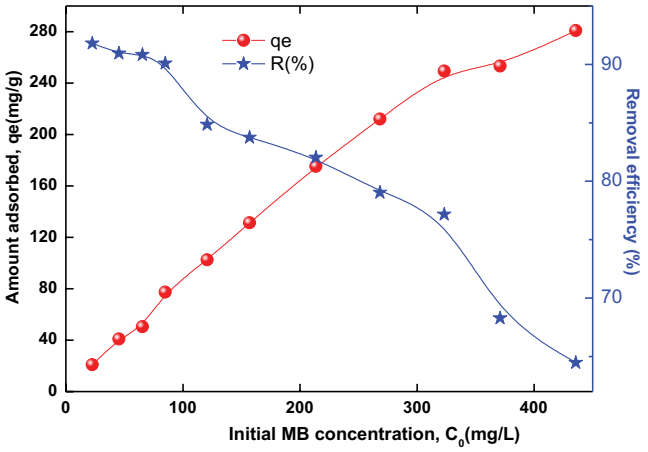

Fig. 5. Effect of initial concentration of methylene blue.

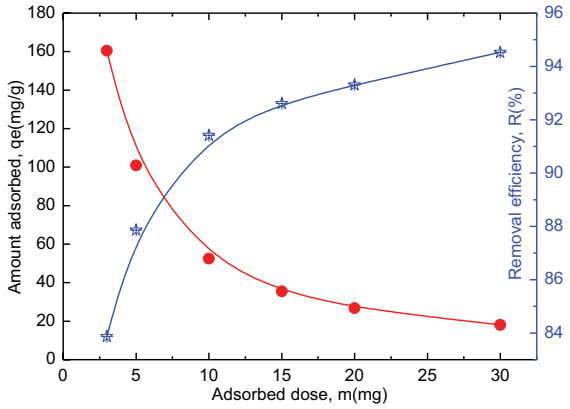

Fig. 6. Effect of black cumin seed waste dose on the adsorbed amount and percentage removal of methylene blue dye.

The purpose of the ionic strength effect study is to test the adsorption efficiency of MB on BSW using competing ions in solution. The experiments were performed with NaCl concentrations ranging from 0 to 10^{-1} mol/L, pH = 6.4 > pH_{PZC}, adsorbent dose of 20 mg, contact time of 2 h and MB dye solution concentration of 57.4 mg/L (Figure not shown). It is observed that the adsorbed amount q_e of MB decreases from 52.36 to 35.6 mg/g when the ionic strength increases from 0 to 10^{-1} mol/L. These results are attributed to the competition effect between MB^+ and Na^+ ions for the negatively charged sites located on surface [2].

3.3. Kinetics of adsorption

The effect of the contact time of MB adsorption on BSW was studied for three different initial concentrations 7.8, 32.19 and 56.5 mg/L at pH 6.4. Fig. 7 presents the results of adsorbed quantity in MB at time t (q_t) as a function of time t (0–2 h). It was indicated that the equilibrium time depending on the initial concentration in MB; 10 min for concentrations 7.8 and 32.19 mg/L and 20 min for concentration 56.5 mg/L. It can be seen that the adsorption is rapid during the first minutes of the process. This can be interpreted by the fact that at the beginning of adsorption, the number of active sites available on the surface of the adsorbent is much greater than that of the sites remaining after a certain time. Since, after saturation of the sites located on the surface of the adsorbent, the dye molecule needs time to diffuse inside the surface of the adsorbent [2].

Two kinetic models were used to interpret the experimental data. Non-linear forms of pseudo-first-order and pseudo-second-order [45] kinetic equations are described in Eqs. (6) and (7), respectively.

$$q_t = q_e\left(1 - e^{-k_1 t}\right) \tag{4}$$

$$q_t = \frac{k_2 \times q_e^2 \times t}{1 + k_2 \times q_e \times t} \tag{5}$$

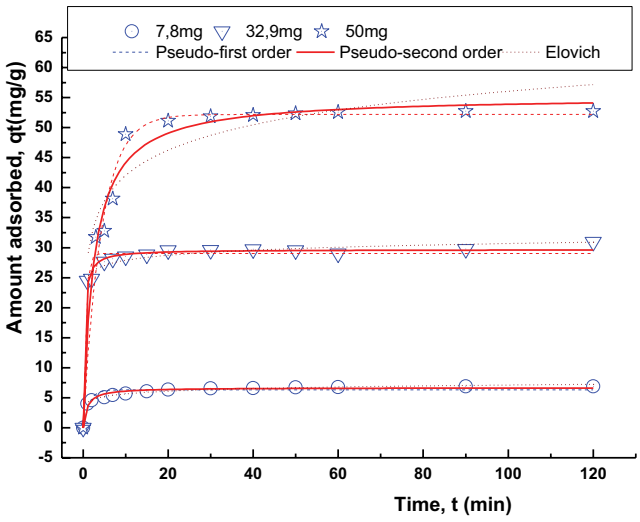

Fig. 7. Adsorption capacity of methylene blue onto black cumin seed waste vs. contact time and initial dye concentration.

where the amounts of MB adsorbed at time t and at equilibrium, expressed in mg/g, are denoted by the variables q_t and q_e, respectively. The rate constants for the pseudo-first-order and pseudo-second-order models, respectively, are k_1 (min^{-1}) and k_2 (g/mg·min). Fig. 7 depicts the kinetic models' non-linear fitted results for the adsorption of MB onto BSW. The kinetic parameters of the different models are summarized in Table 1. According to the R^2 and $AIC_{corrected}$ values, the pseudo-second-order model showed the highest correlation coefficient (R^2) and the lowest $AIC_{corrected}$. In addition, the quantities of MB adsorbed at equilibrium calculated with the pseudo-second-order model (q_e) are close to experimental values ($q_{e,exp}$). This indicates that the pseudo-second-order model was best at describing the experimental data. According to the literature, the pseudo-second-order kinetic model assumes that the rate-limiting stage is chemical adsorption, which comprises the transmission of electrons between the adsorbent and the adsorbate [46]. Several studies have reported that the pseudo-second-order model has been successfully used to represent experimental kinetics data for MB adsorption on various adsorbents [25,38,47]. Besides, the models of intraparticle diffusion and film diffusion have also been used to understand the adsorption mechanism expressed through Eqs. (8) and (9), respectively [48]:

$$q_t = K_3 \times t^{0.5} + C \tag{6}$$

$$-\ln\left(\frac{q_e - q_t}{q_e}\right) = K_4 \times t \tag{7}$$

Table 1
Kinetic model parameters

C_0 (mg/L)	7.8	32.19	56.5
$q_{e,exp}$ (mg/g)	6.7	31.0	52.7
Pseudo-first-order model			
q_e (mg/g)	6.31	29.04	52.2
k_1 (min^{-1})	0.754	1.61	0.23
R^2	0.901	0.938	0.976
$AIC_{corrected}$	–9.2	12.9	28.1
Pseudo-second-order model			
q_e (mg/g)	6.7	29.7	55.2
k_2 (g/mg·min)	0.16	0.125	0.007
R^2	0.970	0.992	0.977
$AIC_{corrected}$	–26.0	–3.8	27.4
Intraparticle diffusion model			
K_3 (mg/g·min$^{0.5}$)	0.42	1.4	3.6
C	3.6	20.0	24.6
R^2	0.534	0.272	0.539
Film diffusion model			
K_4 (min^{-1})	0.109	0.004	0.130
R^2	0.985	0.967	0.852

where K_3 (mg/g·min$^{0.5}$) is the constant of the intraparticle diffusion rate, C (mg/g) is the boundary layer thickness and K_4 (min^{-1}) is the constant of the liquid film diffusion. According to the plots of q_t vs. $\sqrt{t}$ (Fig. 8), there are two straight lines, indicating two steps occur in the adsorption of MB onto BSW. The first step in the period of $\sqrt{t} < 3$ is the adsorption at the external surface. The second step, in the range of $3 \le \sqrt{t} \le 11$, is the progressive adsorption of MB until reaching the equilibrium of the process. In addition, q_t vs. $\sqrt{t}$ not pass through the origin, (C (mg/g) (the thickness of the boundary layer) is not zero), which indicates that diffusion was not simply a rate-determining process. Furthermore, the Boyd graphs are linear but do not pass through the origin, describing how the adsorption rate is influenced by the film diffusion mechanism. Similarly, when the data in Table 1 were compared, the intraparticle diffusion model had a lower R^2 than the film diffusion model. Therefore, the MB adsorption on the surface of BSW was controlled by the film diffusion step.

3.4. Adsorption isotherms

Fig. 9 depicts the adsorption isotherm of MB onto the BSW surface. We notice that the shape of the isotherm is of type L according to the classification of Limousin et al. [49]. This isotherm indicates that adsorption becomes more difficult when the degree of coverage of the surface increases. This behavior is observed in the case where the adsorption of the solvent is weak, and when the molecules are not oriented vertically, but rather flat. This isotherm indicates that MB has a high affinity for BSW surface, especially at low concentrations. The two-parameter (Langmuir, Freundlich, and Temkin) and three-parameter (Sips, Toth, and Redlich–Peterson) non-linear models were used to elucidate the mechanism of adsorption [50].

$$q_e = \frac{q_m \times K_L \times C_e}{1 + K_L \times C_e} \tag{8}$$

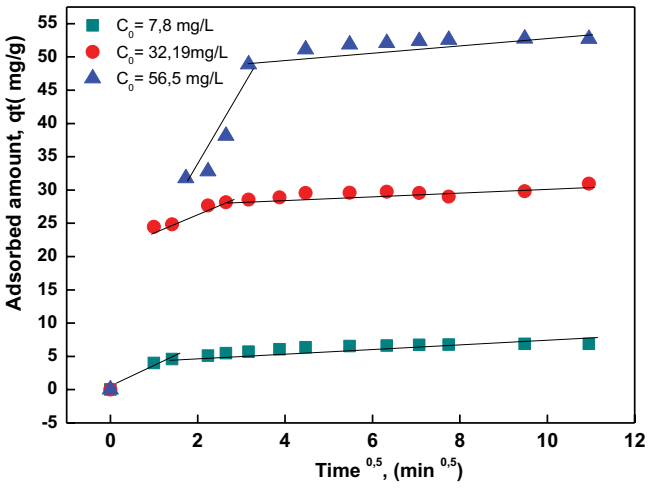

Fig. 8. Intraparticle diffusion model of the adsorption of methylene blue on black cumin seed waste.

$$q_e = K_F \times C_e^{1/n} \tag{9}$$

$$q_e = \frac{R \times T}{b_T} \times \ln\left(A_T \times C_e\right) \tag{10}$$

$$q_e = \frac{q_m \times K_s \times C_e^{\mathrm{ms}}}{1 + K_s \times C_e^{\mathrm{ms}}} \tag{11}$$

$$q_e = \frac{q_m \times K_T \times C_e}{\left(1 + \left(K_T \times C_e\right)^{n_f}\right)^{1/n_f}} \tag{12}$$

$$q_e = \frac{A_{\mathrm{RP}} \times C_e}{1 + B_{\mathrm{RP}} \times C_e^{g}} \tag{13}$$

$$R_L = \frac{1}{\left(1 + K_L C_0\right)} \tag{14}$$

where q_m (mg/g) represent the maximum adsorption capacity of the adsorbent, K_L (dm^3/mg) is the affinity constant, K_F in (mg/g)(L/mg)$^{1/n}$ and n are the Freundlich constants, b_T (kJ/mol) and A_T (L/mol) are the Temkin constants, R (J/mol·K) is the universal gas constant, T (K) is the temperature, K_s (L/g)$^{\mathrm{ns}}$ and n_s are Sips constants. A_{RP} (L/g) and B_{RP} (L^g/mg^g) are the constants of Redlich–Peterson, g is the exponent ($0 = g \le 1$), K_T (L/mg) and n_T are Toth constants, R_L is the separator factor. The constants parameters (R^2 and AIC$_{\mathrm{corrected}}$), determined for non-linear Langmuir, Freundlich, Temkin, Sips, Toth, and Redlich–Peterson models are recorded in Table 2. The values of the separation factor R_L ($0.1 < R_L < 0.38$) of Langmuir and the parameter n of the Freundlich models, known as the adsorption intensity, ($1/n$ = 0.432) indicate the favorable and physical process of MB adsorption onto BSW [51]. Beside, by correlating the R^2 and AIC$_{\mathrm{corrected}}$ values of the isothermal adsorption models, the adsorption data are well suitable with the Langmuir (R_L^2 = 0.994, AIC$^{L}_{\mathrm{corrected}}$ = 56.68) followed by Freundlich (R_L^2 = 0.994, AIC$^{\mathrm{Fr}}_{\mathrm{corrected}}$ = 61.74), Temkin (R_L^2 = 0.969, AIC$^{\mathrm{Temkin}}_{\mathrm{corrected}}$ = 80.5), Toth (R^2_{Th} = 0.994, AIC$^{\mathrm{To}}_{\mathrm{corrected}}$ = 63.11), Sips (R^2_{Sp} = 0.995, AIC$^{\mathrm{Sips}}_{\mathrm{corrected}}$ = 61.74) and then Redlich–Peterson (R_L^{RP} = 0.994, AIC$^{\mathrm{RP}}_{\mathrm{corrected}}$ = 63.1). In addition, n_s (=0.92), n_T (=0.97) and g (=0.969) constants values, respectively for Sips, Toth and Redlich–Peterson are very close to 1, which confirm the MB adsorption process occurs in a homogeneous system and is likely to follow the Langmuir model [50]. The values of q_m obtained with the Langmuir, Sips and Toth models are 346.1, 366.3 and 317.41 mg/g, respectively. In Table 3, we have recorded the maximum adsorption capacities and experimental conditions of MB adsorption on the different adsorbents. The high capacity of our bioadsorbent shows that this material can be used for micropollutants removal.

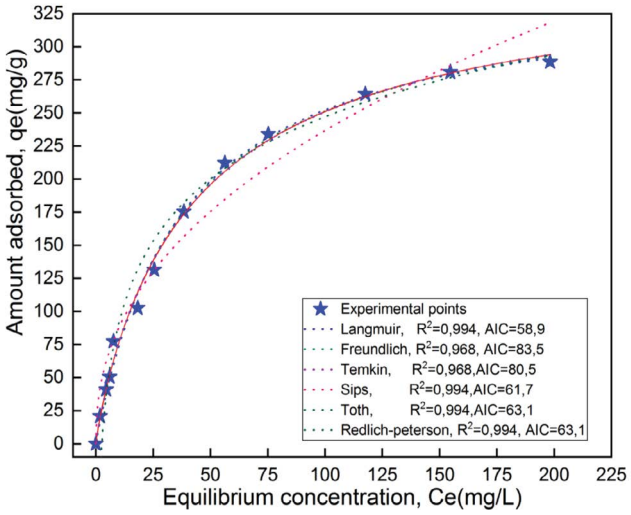

Fig. 9. Adsorption isotherm of methylene blue on black cumin seed waste.

3.5. Statistical physics model

In Section 3.4 – Adsorption isotherms we displayed that the Langmuir model best describes the adsorption isotherm, but it ignores lateral interactions between adsorbed molecules and proposes that each site can bind a single molecule. According to the following equation, another statistical physics-based model suggests that each site can accept n molecules [52].

$$q_e = \frac{n \times D_m}{1 + \left(C_{1/2} / C_e\right)^n} \tag{15}$$

$$\mathrm{Ou}: N_{\mathrm{sat}} = n \times D_m \tag{16}$$

where n designates the number of MB dye molecules adsorbed on the BSW surface per functional group, D_m

Table 2
Isotherm model parameters

Two-parameter isotherm models			Three-parameter isotherm models		
Langmuir	Freundlich	Temkin	Sips	Toth	Redlich–Peterson
q_m = 346.1	K_F = 32.39	A_T = 0.44	q_m = 366.3	q_m = 317.41	A_{RP} = 9.77
K_L = 0.027	n_f = 0.432	b_T = 38.6	K_s = 0.032	K_T = 0.03	B_{RP} = 0.033
			n_s = 0.92	n_T = 0.97	g = 0.969
R^2 = 0.994	R^2 = 0.968	R^2 = 0.969	R^2 = 0.994	R^2 = 0.994	R^2 = 0.994
AICc = 62.1	AICc = 86.7	AICc = 83.7	AICc = 67.7	AICc = 69.1	AICc = 69.1

q_m (mg/g), K_L (L/mg), K_F (mg/g)(L/mg)$^{1/n}$), A_T (L/mol), b_T (kJ/mol), K_s (L/g)^{n_s}, K_T (L/mg), A_{RP} (L/g), B_{RP} (L^g/mg^g).

Table 3
Comparison of maximum monolayer adsorption capacity on various adsorbents

Adsorbents	Concentrations initial	q_m (mg/g)	References
Castor seed shell	C_0 = 25–300 mg/L	158	[56]
Waste seeds *Aleurites moluccana*	C_0 = 50–300 mg/L	178	[57]
Dragon fruit speels	C_0 = 50–400 mg/L	192.3	[7]
Cucumis sativus speels	C_0 = 25–250 mg/L	21.5	[58]
Cucumeropsis mannii Naudin waste seeds	C_0 = 1–100 mg/L	47	[59]
Nerium oleander, *Pergularia tomentosa* and *Populus tremula* seeds	C_0 = 10–60 mg/L	280.2 168	[60]
Moringa oleifera seed husks	C_0 = 5–90 mg/L	122.7	[61]
Black cumin seed waste	C_0 = 10–500 mg/L	346.1	This work

(mg/g) denotes the density of BSW functional groups engaged in dye adsorption, and $C_{1/2}$ indicates the corresponding half saturation concentration (mg/L). (N_{sat}) is the amount of dye adsorbed at saturation. The number n, according to the literature [53], shows the location of adsorbed molecules on the adsorbent's surface. The model and the observational results have a similar trend, as indicated by the R^2 value (=0.995), with n = 0.92.This value indicates the number of MB molecules adsorbed per functional group of the BSW bioadsorbent and indicates MB molecules are parallel oriented and fixed to BSW [53]. D_m was 396.3 mg/g for the density of functional groups implicated in MB adsorption.

3.6. Thermodynamics of adsorption

The thermodynamic parameters such as a change in Gibbs free energy (Δ*G*, kJ/mol), change in enthalpy (Δ*H*, kJ/mol), and change in entropy (Δ*S*, J/mol) for MB adsorption were estimated using the following equations [54]:

$$\Delta G = -RT\ln K \tag{17}$$

$$\log\left(\frac{1000\times q_e}{C_e}\right) = \frac{-\Delta H}{2.303RT} + \frac{\Delta S}{2.303R} \tag{18}$$

where R and K are ideal gas constant and equilibrium constant, respectively.

The values of Δ*H* reveal that the MB adsorption mechanism on BSW is exothermic preferring low temperatures (Table 4). While Δ*S* is negative, it suggests that the disorder at the solid-solution interface is declining. The negative Δ*G* value means that the process is spontaneous and desirable. This decrease in adsorption capacity is probably due to a decrease in hydrogen bond strength or biosorbent degradation [55].

Table 4
Thermodynamic parameters

T (K)	Δ*H* (kJ/mol)	Δ*S* (J/mol·K)	ΔG (kJ/mol)
293			–14.50
303	–18.13	–12.45	–14.35
313			–14.23

4. Theoretical investigation

4.1. Equilibrium configurations

In the most common version, Molecular Dynamics Simulation (MDS) is a computational method for investigating the motions of molecules. For a predetermined period of time, the molecules are permitted to interact, illustrating a view of the system's evolution. In our work, MDS has been used to find the macroscopic configuration of the adsorption system through the minimization of the energy for each adsorption site. The equilibrium configurations of the adsorbed MB and water molecules on cellulose shown the exterior atomic layer was used for the adsorption. According to the equilibrium configurations, it is observed that MB is adsorbed through the aromatic ring, with an average interspacing of 2.85 Å, at this distance; MB interaction can be physico-chemical. The co-adsorption of MB with water molecules differs from that without water, declaring that the water molecules may occupy the adsorption sites of MB molecules.

The associated output adsorption energies (with the substrate energy set to null) are summarized in Table 5, with the total, stiff adsorption and deformation energies, and dEads/dNi. The physical description of these energies was reported earlier [32]; their negative values point out the spontaneity of the adsorption.

4.2. Adsorption mechanism discussion

The adsorption mechanism is the consequence of the interaction between the solid surface and the structure of dye molecules. The width, depth, and thickness of the MB molecule were previously determined to be 1.43, 0.61, and 0.4 nm, respectively [62]. These dimensions enable this molecular dye to conveniently penetrate the 14.1 nm-diameter holes of BSW's porous structure. Besides, surface functional groups such as hydroxyl (–OH), carbonyl (–C=O), carboxyl (–COOH), and amine (–NH_2) groups, as well as the charge of the MB molecule, which is likely localized on the nitrogen atoms, significantly affect the adsorption process. The FTIR spectrum after MB adsorption by BSW sample indicated the appearance of new absorption peaks attributed to the MB molecules. Moreover, the adsorption process was performed at pH > pH_{PZC}, in which electrostatic

Table 5
Adsorption energies of the methylene blue and the water molecules onto BSW surface

	Total energy	Adsorption energy	Rigid adsorption energy	Deformation energy	MB dEad/dNi	Water dEad/dNi
MB/BSW	30.41	–46.87	–31.59	–15.28	–46.87	/
Water/BSW	–2.78	–4.244	–2.78	–1.47	/	–4.25
MB-water/BSW	–79.27	–215.28	–141.26	–74.03	–55.01	–3.82

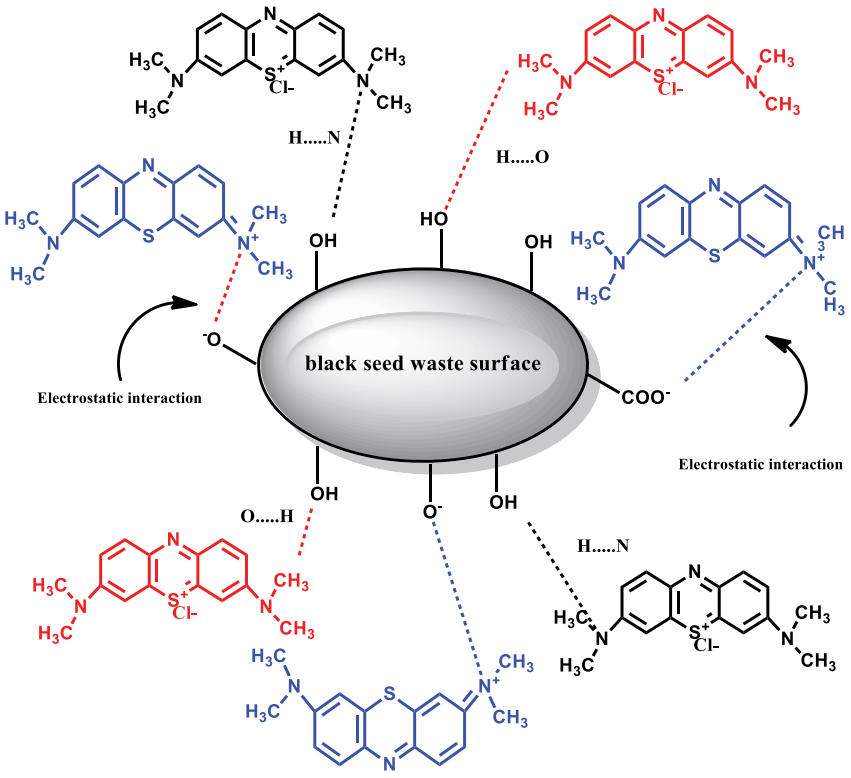

Fig. 10. Suggested adsorption mechanism.

interactions between the surface's negative charge and the MB^+ cations predominate. The various mechanisms proposed are shown in Fig. 10.

- Electrostatic interactions: (1) between the negatively charged deprotonated carboxylate anions of BSW and the positive charges located on the MB nitrogen atoms and (2) between the density of delocalized electrons of the aromatic rings of the MB and the hydrogen atoms.
- Hydrogen bonds: between the hydrogen of the hydroxyl groups of the BSW and the oxygen atoms of the surface.

5. Conclusion

The present work explored the efficacy of black cumin seed waste (BSW) as an alternative biosorbent for the removal of methylene blue (MB) dye from aqueous solutions. The results demonstrated that under varying solution conditions including pH, temperature, biosorbent dosage, ionic strength and initial dye concentration, BSW exhibited promising MB adsorption capabilities. Furthermore, the Langmuir isotherm model provided the best fit for the equilibrium adsorption data based on the lowest AIC value, with a maximum monolayer adsorption capacity of 346.1 mg/g. The pseudo-second-order kinetic model was found to suitably describe the dynamic adsorption process compared to the pseudo-first-order model. Thermodynamic analysis indicated the adsorption reaction to be spontaneous and exothermic in nature based on the negative values of Gibbs free energy change (ΔG) and enthalpy change (ΔH). FTIR analysis of BSW, MB and MB-adsorbed BSW suggested the involvement of functional groups such as carboxyl, hydroxyl and amine groups in the adsorption mechanism. SEM imaging revealed the horizontal orientation of MB molecules on the biosorbent surface. The adsorption process appeared to be governed by multiple mechanisms including electrostatic interactions, van der Waals forces and hydrogen bonding, as corroborated by molecular docking studies. Overall, this study demonstrates BSW to be a

promising low-cost biosorbent for the efficient removal of MB dye from wastewaters at large scale. The abundant availability and biodegradable nature of BSW further reinforces its potential as an environmentally sustainable adsorbent for dye removal applications.

Declaration of competing interest

The authors report no conflicts of interest.

Credit authorship contributions statement

Faouzia Benamraoui: conceptualization, methodology, formulations, writing, experimental, writing, software. Riad Bourzami: writing, supervision, software. Boudiaf Hassina: writing, review, Bouhank Antar: software, Bencheikh Lahcene: Review, Antonio Gil: supervision, review, Boulahbal Aziza Imene: experimental, Mokhtar Boutahala: conceptualization supervision, writing, review.

References

[1] J. Mittal, Permissible synthetic food dyes in India, Resonance, 25 (2020) 567–577.
[2] C. Arora, P. Kumar, S. Soni, J. Mittal, A. Mittal, B. Singh, Efficient removal of malachite green dye from aqueous solution using *Curcuma caesia* based activated carbon, Desal. Water Treat., 195 (2020) 341–352.
[3] J. Mittal, A. Mariyam, F. Sakina, R.T. Baker, A.K. Sharma, A. Mittal, Batch and bulk adsorptive removal of anionic dye using metal/halide-free ordered mesoporous carbon as adsorbent, J. Cleaner Prod., 321 (2021) 129060, doi: 10.1016/j.jclepro.2021.129060.
[4] A. Mariyam, J. Mittal, F. Sakina, R.T. Baker, A.K. Sharma, A. Mittal, Efficient batch and fixed-bed sequestration of a basic dye using a novel variant of ordered mesoporous carbon as adsorbent, Arabian J. Chem., 14 (2021) 103186, doi: 10.1016/j.arabjc.2021.103186.
[5] A.H. Jawad, R.A. Rashid, R.M. Mahmuod, M.A.M. Ishak, N.N. Kasim, K. Ismail, Adsorption of methylene blue onto coconut (*Cocos nucifera*) leaf: optimization, isotherm and kinetic studies, Desal. Water Treat., 57 (2016) 8839–8853.
[6] H. Daraei, A. Mittal, Investigation of adsorption performance of activated carbon prepared from waste tire for the removal of methylene blue dye from wastewater, Desal. Water Treat., 90 (2017) 294–298.
[7] A.H. Jawad, A.M. Kadhum, Y.S. Ngoh, Applicability of dragon fruit (*Hylocereus polyrhizus*) peels as low-cost biosorbent for adsorption of methylene blue from aqueous solution: kinetics, equilibrium and thermodynamics studies, Desal. Water Treat., 109 (2018) 231–240.
[8] S. Rahmani, B. Zeynizadeh, S. Karami, Removal of cationic methylene blue dye using magnetic and anionic-cationic modified montmorillonite: kinetic, isotherm and thermodynamic studies, Appl. Clay Sci., 184 (2020) 105391, doi: 10.1016/j.clay.2019.105391.
[9] Y. Zhou, J. Lu, Y. Zhou, Y. Liu, Recent advances for dyes removal using novel adsorbents: a review, Environ. Pollut., 252 (2019) 352–365.
[10] M. Kadhom, N. Albayati, H. Alalwan, M. Al-Furaiji, Removal of dyes by agricultural waste, Sustainable Chem. Pharm., 16 (2020) 100259, doi: 10.1016/j.scp.2020.100259.
[11] L. Zafar, A. Khan, U. Kamran, S.-J. Park, H.N. Bhatti, Eucalyptus (camaldulensis) bark-based composites for efficient Basic Blue 41 dye biosorption from aqueous stream: kinetics, isothermal, and thermodynamic studies, Surf. Interfaces, 31 (2022) 101897, doi: 10.1016/j.surfin.2022.101897.
[12] J. Mittal, R. Ahmad, A. Mittal, Kahwa tea (*Camellia sinensis*) carbon — a novel and green low-cost adsorbent for the sequestration of titan yellow dye from its aqueous solutions, Desal. Water Treat., 227 (2021) 404–411.
[13] A. Mittal, R. Jain, S. Varshney, S. Sikarwar, J. Mittal, Removal of Yellow ME 7 GL from industrial effluent using electrochemical and adsorption techniques, Int. J. Environ. Pollut., 43 (2010) 308–323.
[14] R. Subramaniam, S. Kumar Ponnusamy, Novel adsorbent from agricultural waste (cashew NUT shell) for methylene blue dye removal: optimization by response surface methodology, Water Res. Ind., 11 (2015) 64–70.
[15] A. Mittal, J. Mittal, L. Kurup, A.K. Singh, Process development for the removal and recovery of hazardous dye erythrosine from wastewater by waste materials—bottom ash and de-oiled soya as adsorbents, J. Hazard. Mater., 138 (2006) 95–105.
[16] V. Ponnusami, S. Vikram, S.N. Srivastava, Guava (*Psidium guajava*) leaf powder: novel adsorbent for removal of methylene blue from aqueous solutions, J. Hazard. Mater., 152 (2008) 276–286.
[17] A. Patel, S. Soni, J. Mittal, A. Mittal, C. Arora, Sequestration of crystal violet from aqueous solution using ash of black turmeric rhizome, Desal. Water Treat., 220 (2021) 342–352.
[18] L. Kong, L. Gong, J. Wang, Removal of methylene blue from wastewater using fallen leaves as an adsorbent, Desal. Water Treat., 53 (2015) 2489–2500.
[19] R.R. Krishni, K.Y. Foo, B.H. Hameed, Adsorption of cationic dye using a low-cost biowaste adsorbent: equilibrium, kinetic, and thermodynamic study, Desal. Water Treat., 52 (2014) 6088–6095.
[20] R.R. Krishni, K.Y. Foo, B.H. Hameed, Adsorptive removal of methylene blue using the natural adsorbent-banana leaves, Desal. Water Treat., 52 (2014) 6104–6112.
[21] A. Khabbazi, Z. Javadivala, N. Seyedsadjadi, A. Malek Mahdavi, A systematic review of the potential effects of *Nigella sativa* on Rheumatoid Arthritis, Plant. Med., 86 (2020) 457–469.
[22] M. Mahboubi, Natural therapeutic approach of *Nigella sativa* (black seed) fixed oil in management of Sinusitis, Integr. Med. Res., 7 (2018) 27–32.
[23] P.M. Thabede, N.D. Shooto, T. Xaba, E.B. Naidoo, Adsorption studies of toxic cadmium(II) and chromium(VI) ions from aqueous solution by activated black cumin (*Nigella sativa*) seeds, J. Environ. Chem. Eng., 8 (2020) 104045, doi: 10.1016/j.jece.2020.104045.
[24] N.D. Shooto, P.M. Thabede, E.B. Naidoo, Simultaneous adsorptive study of toxic metal ions in quaternary system from aqueous solution using low-cost black cumin seeds (*Nigella sativa*) adsorbents, S. Afr. J. Chem. Eng., 30 (2019) 15–27.
[25] S.I. Siddiqui, G. Rathi, S.A. Chaudhry, Acid washed black cumin seed powder preparation for adsorption of methylene blue dye from aqueous solution: thermodynamic, kinetic and isotherm studies, J. Mol. Liq., 264 (2018) 275–284.
[26] P.M. Thabede, N.D. Shooto, Application of black cumin (*Nigella sativa* L.) seeds for the removal of metal ions and methylene blue from aqueous solutions, Cogent Eng., 9 (2022) 2013419, doi: 10.1080/23311916.2021.2013419.
[27] S. Brunauer, P.H. Emmett, E. Teller, Adsorption of gases in multimolecular layers, J. Am. Chem. Soc., 60 (1938) 309–319, doi: 10.1021/ja01269a023.
[28] S.I. Siddiqui, S.A. Chaudhry, *Nigella sativa* plant-based nanocomposite-$MnFe_2O_4$/BC: an antibacterial material for water purification, J. Cleaner Prod., 200 (2018) 996–1008.
[29] X. Guo, Y. Liu, J. Wang, Sorption of sulfamethazine onto different types of microplastics: a combined experimental and molecular dynamics simulation study, Mar. Pollut. Bull., 145 (2019) 547–554.
[30] Y. Nishiyama, P. Langan, H. Chanzy, Crystal structure and hydrogen-bonding system in cellulose Iβ from synchrotron x-ray and neutron fiber diffraction, J. Am. Chem. Soc., 124 (2002) 9074–9082.
[31] R. Bourzami, L. Ouksel, N. Chafai, Synthesis, spectral analysis, theoretical studies, molecular dynamic simulation and comparison of anticorrosive activity of an ester and an acid α-hydroxyphosphonates, J. Mol. Struct., 1195 (2019) 839–849.

[32] D. Sid, M. Baitiche, R. Bourzami, R. Merir, F. Djerboua, A. Gil, M. Boutahala, Experimental and theoretical studies of the interaction of ketoprofen in halloysite nanotubes, Colloids Surf., A, 627 (2021) 127136, doi: 10.1016/j.colsurfa.2021.127136.
[33] M. Radjai, H. Ferkous, Z. Jebali, H. Majdoub, R. Bourzami, G. Raffin, M. Achour, A. Gil, M. Boutahala, Adsorptive removal of cationic and anionic dyes on a novel mesoporous adsorbent prepared from diatomite and anionic cellulose nanofibrils: experimental and theoretical investigations, J. Mol. Liq., 361(2022) 119670, doi: 10.1016/j.molliq.2022.119670.
[34] L.E. Torres-Sánchez, G. Berkowitz, L. López-Carrillo, L. Torres-Arreola, C. Ríos, M. López-Cervantes, Intrauterine lead exposure and preterm birth, Environ. Res., 81 (1999) 297–301.
[35] C. Djilani, R. Zaghdoudi, A. Modarressi, M. Rogalski, D. Faycal, A. Lallam, Elimination of organic micropollutants by adsorption on activated carbon prepared from agricultural waste, Chem. Eng. J., 189–190 (2012) 203–212.
[36] A.H. Jawad, A. Kadhum, Y. Ngoh, Applicability of dragon fruit (*Hylocereus polyrhizus*) peels as low-cost biosorbent for adsorption of methylene blue from aqueous solution: kinetics, equilibrium and thermodynamics studies, Desal. Water Treat., 109 (2018) 231–240.
[37] M.D.G. de Luna, E.D. Flores, D.A.D. Genuino, C.M. Futalan, M.-W. Wan, Adsorption of Eriochrome Black T (EBT) dye using activated carbon prepared from waste rice hulls—optimization, isotherm and kinetic studies, J. Taiwan Inst. Chem. Eng., 44 (2013) 646–653.
[38] A.K. Kushwaha, N. Gupta, M.C. Chattopadhyaya, Removal of cationic methylene blue and malachite green dyes from aqueous solution by waste materials of *Daucus carota*, J. Saudi Chem. Soc., 18 (2014) 200–207.
[39] M. Ghaedi, H. Hossainian, M. Montazerozohori, A. Shokrollahi, F. Shojaipour, M. Soylak, M.K. Purkait, A novel acorn based adsorbent for the removal of brilliant green, Desalination, 281 (2011) 226–233.
[40] A. Nasrullah, B. Saad, A.H. Bhat, A.S. Khan, M. Danish, M.H. Isa, A. Naeem, Mangosteen peel waste as a sustainable precursor for high surface area mesoporous activated carbon: characterization and application for methylene blue removal, J. Cleaner Prod., 211 (2019) 1190–1200.
[41] Y. Zhou, J. Lu, Y. Zhou, Y. Liu, Recent advances for dyes removal using novel adsorbents: a review, Environ. Pollut., 252 (2019) 352–365.
[42] L. Hevira, Zilfa, Rahmayeni, J.O. Ighalo, H. Aziz, R. Zein, *Terminalia catappa* shell as low-cost biosorbent for the removal of methylene blue from aqueous solutions, J. Ind. Eng. Chem.,97 (2021) 188–199.
[43] S. Noreen, H.N. Bhatti, M. Iqbal, F. Hussain, F.M. Sarim, Chitosan, starch, polyaniline and polypyrrole biocomposite with sugarcane bagasse for the efficient removal of Acid Black dye, Int. J. Biol. Macromol., 147 (2020) 439–452.
[44] M.D.G. de Luna, E.D. Flores, D.A.D. Genuino, C.M. Futalan, M.-W. Wan, Adsorption of Eriochrome Black T (EBT) dye using activated carbon prepared from waste rice hulls—optimization, isotherm and kinetic studies, J. Taiwan Inst. Chem. Eng., 44 (2013) 646–653.
[45] J. Wang, X. Guo, Adsorption kinetic models: physical meanings, applications, and solving methods, J. Hazard. Mater., 390 (2020) 122156, doi: 10.1016/j.jhazmat.2020.122156.
[46] S. Sahnoun, M. Boutahala, Adsorption removal of tartrazine by chitosan/polyaniline composite: kinetics and equilibrium studies, Int. J. Biol. Macromol., 114 (2018) 1345–1353.
[47] S. Rakass, A. Mohmoud, H. Oudghiri Hassani, M. Abboudi, F. Kooli, F. Al Wadaani, Modified *Nigella sativa* seeds as a novel efficient natural adsorbent for removal of methylene blue dye, Molecules, 23 (2018) 1950, doi: 10.3390/molecules23081950.
[48] A. Benhouria, Md. A. Islam, H. Zaghouane-Boudiaf, M. Boutahala, B.H. Hameed, Calcium alginate–bentonite–activated carbon composite beads as highly effective adsorbent for methylene blue, Chem. Eng. J., 270 (2015) 621–630.
[49] G. Limousin, J.-P. Gaudet, L. Charlet, S. Szenknect, V. Barthès, M. Krimissa, Sorption isotherms: a review on physical bases, modeling and measurement, Appl. Geochem., 22 (2007) 249–275.
[50] N.B. Singh, G. Nagpal, S. Agrawal, Rachna, Water purification by using adsorbents: a review, Environ. Technol. Innovation, 11 (2018) 187–240.
[51] H. Javadian, M.T. Angaji, Mu. Naushad, Synthesis and characterization of polyaniline/γ-alumina nanocomposite: a comparative study for the adsorption of three different anionic dyes, J. Ind. Eng. Chem., 20 (2014) 3890–3900.
[52] L. Sellaoui, G.L. Dotto, E. Ch. Peres, Y. Benguerba, É.C. Lima, A. Ben Lamine, A. Erto, New insights into the adsorption of crystal violet dye on functionalized multi-walled carbon nanotubes: experiments, statistical physics and COSMO–RS models application, J. Mol. Liq., 248 (2017) 890–897.
[53] K.H. Toumi, Y. Benguerba, A. Erto, G.L. Dotto, M. Khalfaoui, Ch. Tiar, S. Nacef, A. Amrane, Molecular modeling of cationic dyes adsorption on agricultural Algerian olive cake waste, J. Mol. Liq., 264 (2018) 127–133.
[54] N. Boukhalfa, M. Boutahala, N. Djebri, A. Idris, Kinetics, thermodynamics, equilibrium isotherms, and reusability studies of cationic dye adsorption by magnetic alginate/oxidized multiwalled carbon nanotubes composites, Int. J. Biol. Macromol., 123 (2019) 539–548.
[55] M. Maqbool, H.N. Bhatti, S. Sadaf, M. Mana AL-Anazy, M. Iqbal, Biocomposite of polyaniline and sodium alginate with *Oscillatoria* biomass: a potential adsorbent for the removal of basic blue 41, J. Mater. Res. Technol., 9 (2020) 14729–14741.
[56] N.A. Oladoja, C.O. Aboluwoye, Y.B. Oladimeji, A.O. Ashogbon, I.O. Otemuyiwa, Studies on castor seed shell as a sorbent in basic dye contaminated wastewater remediation, Desalination, 227 (2008) 190–203.
[57] D.L. Postai, C.A. Demarchi, F. Zanatta, D.C.C. Melo, C.A. Rodrigues, Adsorption of rhodamine B and methylene blue dyes using waste of seeds of *Aleurites moluccana*, a low-cost adsorbent, Alexandria Eng. J., 55 (2016) 1713–1723.
[58] S. Shakoor, A. Nasar, Adsorptive treatment of hazardous methylene blue dye from artificially contaminated water using *Cucumis sativus* peel waste as a low-cost adsorbent, Groundwater Sustainable Dev., 5 (2017) 152–159.
[59] K.M. Kifuani, A.K. Mayeko, B.I. Lopaka, P.N. Bokolombe, T.M. Ondngo, G.E. Bakambo, J.M. Lunguya, Kinetic and thermodynamic studies adsorption of methylene blue (MB) in aqueous solution on a bioadsorbent from *Cucumeropsis mannii* Naudin waste seeds, Int. J. Biol. Chem. Sci., 12 (2018) 2412–2423.
[60] N. Sebeia, M. Jabli, A. Ghith, Y. El Ghoul, F.M. Alminderej, *Populus tremula*, *Nerium oleander* and *Pergularia tomentosa* seed fibers as sources of cellulose and lignin for the bio-sorption of methylene blue, Int. J. Biol. Macromol., 121 (2019) 655–665.
[61] C.A. Lopes, C. Roledo, A.G. dos Reis, *Moringa oleifera* seed husks for methylene blue dye adsorption: kinetic, equilibrium, and thermodynamic analyses, Rev. Ambient., 17 (2022) 1–16, doi: 10.4136/ambi-agua.2812.
[62] C. Pelekani, V.L. Snoeyink, Competitive adsorption between atrazine and methylene blue on activated carbon: the 8520 of pore size distribution, Carbon, 38 (2000) 1423–1436.